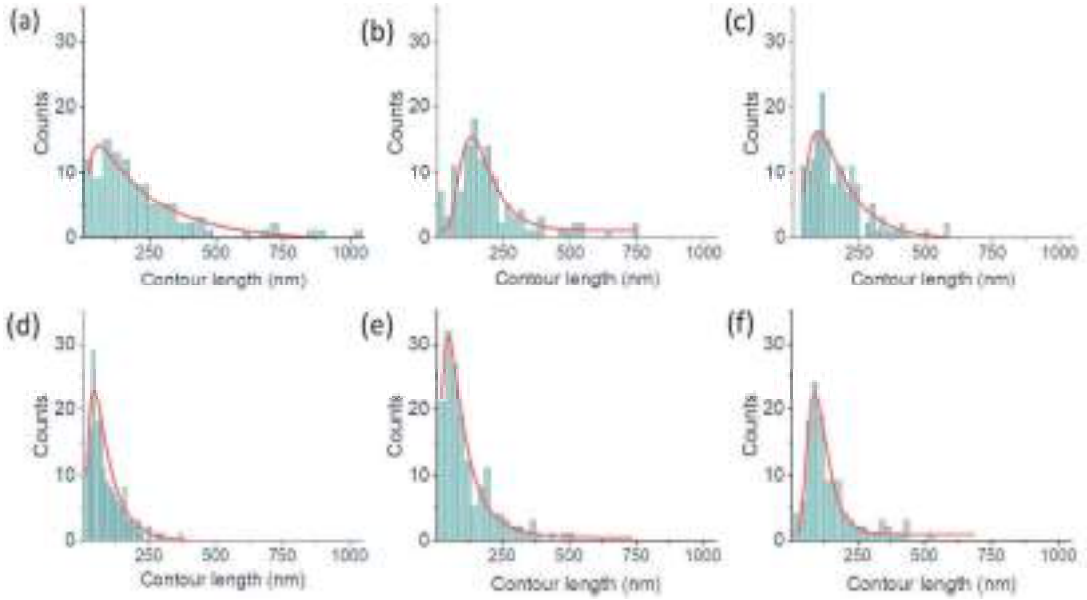

Figure 4. Lamellae length distribution, after annealing, on flat substrate (**a**) and on substrates having different curvatures: 0.00492 nm^{-1} (**b**), 0.00658 nm^{-1} (**c**), 0.00851 nm^{-1} (**d**), 0.0140 nm^{-1} (**e**) and 0.0400 nm^{-1} (**f**), where the contour length is the lengths of the traced lamellae in the AFM phase image, while the count is the number of traced lamellae with that given length. The red lines on different plots represent the log-normal fit of the distributions.

Similarly, the peak of the log-normal fit of the length distribution moves to lower values for curvatures ranging between 0 and 0.00851 nm^{-1}, then remains constant (Figure 5a).

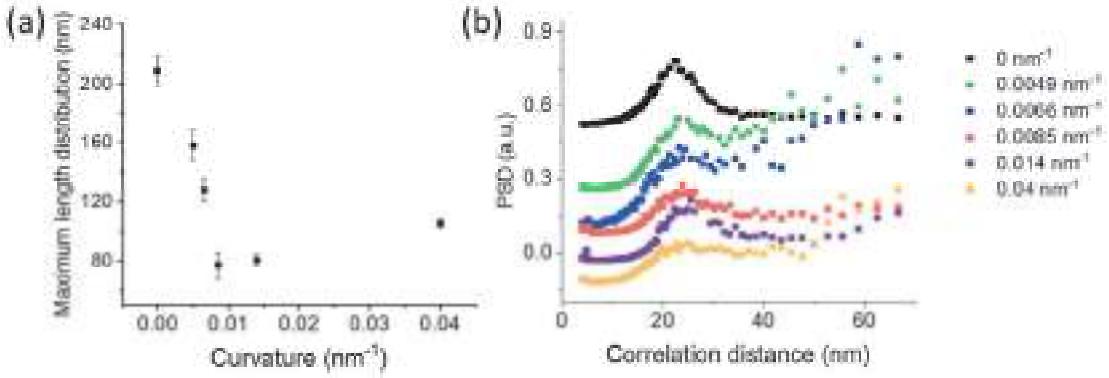

Figure 5. Effect of the surface curvature on the maximum (**a**) of the lamellae length distribution. (**b**) PSD distributions of lamellar thickness of P3HT thin film on substrates having different curvature.

AFM analysis can provide further information on the P3HT crystalline structure by considering the power spectral density (PSD). This tool consists of isotropic Fast Fourier Transform (FFT) filtering, leading to a 1D plot of the reciprocal distance.

Any periodical distance in the AFM images leads to peaks emerging from the sigmoidal PSD plots [34]. In the present case, the periodical signal arises from the constant lamellar thickness generated by the periodic folding of the polymer chain in the crystal [35,36]. Semi-quantitative information was obtained by carrying out a Gaussian fit of the curves (Figure 5b), where the peak position was interpreted as the most probable lamellar thickness. No significant variations in lamellar thickness with curvature were observed, recording mean values of 22.95 $\pm$ 0.8 nm. This constant mean lamellar thickness suggests that the uppermost folded polymer chain lays parallel to the substrate plane.

4. Discussion

The above results demonstrate how nanoscale curvature mostly affects the film crystalline fraction and the crystal size. On the contrary, as revealed by the PSD analysis of the AFM images, the crystal arrangement of the uppermost crystals does not change with the substrate curvature. In the assumption that buried P3HT crystals also arrange in an edge-on orientation, i.e., with the lamellar stacking direction perpendicular to the substrate plane and with the folded chain segments parallel to the substrate, the polymer crystallizes only in those substrate portions where the distance between two neighboring particles is equal or higher than the folding period (L = 22.95 ± 0.8 nm). On the other hand, it is reasonable to assume that the bottom polymer film is amorphous. This leads to a reduction in the crystalline fraction as a function of the surface curvature, which agrees with the reduced intensity of the diffraction peaks on nano-curved substrates and the background increase arising from the short-range ordering of the chain segments (see Figure 1). Moreover, the height "l" required to have a distance between adjacent particles at least equal to the folding period (see Figure 6) changes with the particle radius, i.e., with the substrate curvature, as reported in Figure 6a.

(a)

Curvature (nm^{-1})	l (nm)
0.0049	67.028
0.0066	57.94
0.0085	50.64
0.014	38.85
0.04	21.02

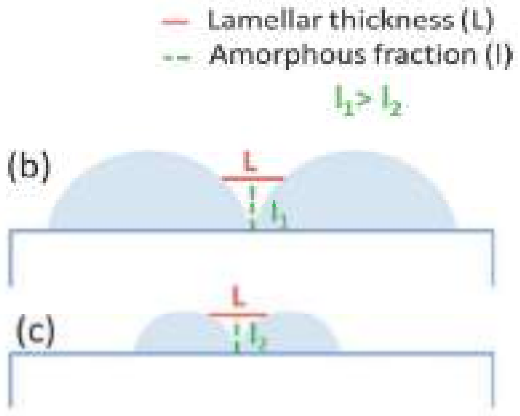

Figure 6. Schematic representation of the nano-curved surface covered by P3HT thin films, where l is the height required to have a distance between adjacent particles at least equal to the folding period L, i.e., the minimum distance between two particles able to accommodate a P3HT lamella. Figures (**b**,**c**) show two different particle dimensions in order to show how l decreases with the reduction of particles diameter leading, as a consequence, to thicker crystallizable film portions above l. (**a**) reported the calculated values of l for all curvatures under investigation.

In particular, as the substrate curvature increases, this height diminishes, causing a corresponding decrease in the polymer fraction that occupies the spaces between neighboring particles. This explains why the broad halo at ~1.7 $Å^{-1}$ decreases at higher curvatures. Moreover, the presence of a larger amorphous fraction (see Figure 6a) also explains why the FWHM of the out-of-plane lamellar stacking peak is higher at lower curvatures, i.e., the out-of-plane crystal size is lower. As a significant fraction of the polymer accumulates in the interstices, the ability of lamellae to grow perpendicularly to the substrate plane is reduced. On the contrary, this reorganization favors the in-plane growth, as confirmed by the AFM images (Figure 3), showing that on low-curvature substrates, more extended crystals formed and, among them, the longest ones grew along the interstices between particles. Vice versa, at higher curvatures, the lower amorphous fraction required to fill the interstices between neighboring particles increases the nucleation probability, leading to many short (thicker) crystals, both in the interstices and on the curved portions of the substrate. Finally, when the film thickness exceeds the particle radius for the 0.04 nm^{-1} substrate, the top crystals nucleate and grow on a flat substrate consisting of particles and an interstice-filling polymer film. This leads back to an increase in the relative edge-on orientation (Figure 2c).

Overall, our results demonstrate that the nanoscale curvature decreases both the crystalline length and out-of-plane thickness, consequently increasing the polymer amorphous fraction. This effect, caused by the amorphous interstice-filling fraction, is markedly dependent on the polymer film thickness, as, for a given curvature, the crystallizable polymer fraction above the threshold thickness "l" increases with the film thickness. As a matter of fact, despite the expected stronger distortive effect played by higher curvatures, polymer films deposited on substrates covered with the smallest particles are characterized, because of the lower threshold thickness, by the highest crystalline fraction. Therefore, we expect that our approach can be extended to thicker polymer films, provided that the appropriate substrate curvature is chosen.

5. Conclusions

We demonstrated how the geometric strain of substrates can be used to modulate the structure of P3HT thin films. The presence of periodic nanoscale curvature influences the crystalline fraction, morphology, and orientation. In particular, the presence of narrow interstices preventing the chain folding required for crystallization reduces the crystalline fraction, this effect being more relevant at lower curvatures. On the other hand, the morphology and orientation of the crystals are dictated by the residual thickness, i.e., the film fraction lying above the threshold distance between two neighboring particles, enabling chain folding. Low residual thicknesses, i.e., low curvatures, favor in-plane crystal growth, leading to longer lamellae characterized by predominant edge-on orientation. Vice versa, on high-curvature substrates, randomly oriented shorter and thicker lamellae form because of the enhanced nucleation and out-of-plane growth.

The reported work provides a novel and easy method to modulate the structure of polymer films by exploiting geometric distortion and interfacial interactions with possible effects on the functional properties of the polymer film. Overall, the reported results could pave the way for subtle management of the morphology and structure control of thin films and to a deeper understanding of the self-assembly behavior of confined soft matter by enabling the quantitative determination of fundamental parameters, such as the crystallization enthalpy and its related loss when nanometric strains are applied. This would allow for greater control of the system and the design of advanced devices, in which it is possible to control the individual building blocks and finely modulate the polymeric assembly. In conclusion, our approach might allow for the creation of devices based on the local control of the properties of the system, where the interactions with the substrate are the key parameters for the realization of finely tailored properties.

Supplementary Materials: The following supporting information can be downloaded at: https://www.mdpi.com/article/10.3390/polym15224453/s1, Figure S1: 1×1 μm^2 AFM height images of flat and nano-curved substrates; Figure S2: 10×10 μm^2 AFM height images of flat and nano-curved substrates.

Author Contributions: Conceptualization, R.R. and G.L.-D.; formal analysis, R.R.; funding acquisition, G.L.-D.; investigation, R.R., M.J., O.K. and G.L.-D.; methodology, R.R. and G.L.-D.; software, R.R.; validation, R.R. and G.L.-D.; writing—original draft, R.R., F.P., N.T. and G.L.-D.; writing—review and editing, M.J. and O.K. All authors have read and agreed to the published version of the manuscript.

Funding: Piano di Incentivi per la Ricerca di Ateneo 2020/2022 (Pia.ce.ri.), Linea 2. MUR-PNRR project SAMOTHRACE (ECS00000022).

Institutional Review Board Statement: Not applicable.

Data Availability Statement: The data presented in this study are available on request from the corresponding author.

Acknowledgments: We acknowledge the European Synchrotron Radiation Facility (ESRF) for providing synchrotron radiation facilities at ID10 surface scattering beamline endstation. GLD acknowledges the Program Piano di Incentivi per la Ricerca di Ateneo 2020/2022 (Pia.ce.ri.), Linea 2, for financial

support. This work has been partially funded by European Union (NextGeneration EU), through the MUR-PNRR project SAMOTHRACE (ECS00000022).

Conflicts of Interest: The authors declare no conflict of interest.

References

1. Joshi, S.; Pingel, P.; Grigorian, S.; Panzner, T.; Pietsch, U.; Neher, D.; Forster, M.; Scherf, U. Bimodal Temperature Behavior of Structure and Mobility in High Molecular Weight P3HT Thin Films. *Macromolecules* **2009**, *42*, 4651–4660. [CrossRef]
2. Roncali, J. Conjugated Poly(Thiophenes): Synthesis, Functionalization, and Applications. *Chem. Rev.* **1992**, *92*, 711–738. [CrossRef]
3. Agbolaghi, S.; Zenoozi, S. A Comprehensive Review on Poly(3-Alkylthiophene)-Based Crystalline Structures, Protocols and Electronic Applications. *Org. Electron.* **2017**, *51*, 362–403. [CrossRef]
4. Nava-Sanchez, R.; Casados-Cruz, G.; Morales-Acevedo, A. Effect of the P3HT Concentration in the Precursor Solution on the Crystallinity of Annealed P3HT Thin Films Prepared by Spin-Coating. In *2022 19th International Conference on Electrical Engineering, Computing Science and Automatic Control (CCE), Mexico City, Mexico, 9–11 November 2022*; IEEE: Mexico City, Mexico, 2022; pp. 1–6.
5. Yu, L.; Davidson, E.; Sharma, A.; Andersson, M.R.; Segalman, R.; Müller, C. Isothermal Crystallization Kinetics and Time–Temperature–Transformation of the Conjugated Polymer: Poly(3-(2′-Ethyl)Hexylthiophene). *Chem. Mater.* **2017**, *29*, 5654–5662. [CrossRef]
6. Crossland, E.J.W.; Rahimi, K.; Reiter, G.; Steiner, U.; Ludwigs, S. Systematic Control of Nucleation Density in Poly(3-Hexylthiophene) Thin Films. *Adv. Funct. Mater.* **2011**, *21*, 518–524. [CrossRef]
7. Tremel, K.; Ludwigs, S. Morphology of P3HT in Thin Films in Relation to Optical and Electrical Properties. In *P3HT Revisited—From Molecular Scale to Solar Cell Devices*; Ludwigs, S., Ed.; Advances in Polymer Science; Springer: Berlin/Heidelberg, Germany, 2014; Volume 265, pp. 39–82.
8. Salammal, S.T.; Mikayelyan, E.; Grigorian, S.; Pietsch, U.; Koenen, N.; Scherf, U.; Kayunkid, N.; Brinkmann, M. Impact of Thermal Annealing on the Semicrystalline Nanomorphology of Spin-Coated Thin Films of Regioregular Poly(3-Alkylthiophene)s as Observed by High-Resolution Transmission Electron Microscopy and Grazing Incidence X-Ray Diffraction. *Macromolecules* **2012**, *45*, 5575–5585. [CrossRef]
9. An, L.; Duan, Y.; Yuan, Y.; Zhou, L.; Zhang, J. Effect of Thermal Annealing on the Microstructure of P3HT Thin Film Investigated by RAIR Spectroscopy. *Vib. Spectrosc.* **2013**, *68*, 40–44. [CrossRef]
10. Yang, H.; Zhang, R.; Wang, L.; Zhang, J.; Yu, X.; Liu, J.; Xing, R.; Geng, Y.; Han, Y. Face-On and Edge-On Orientation Transition and Self-Epitaxial Crystallization of All-Conjugated Diblock Copolymer. *Macromolecules* **2015**, *48*, 7557–7566. [CrossRef]
11. Kim, D.H.; Jang, Y.; Park, Y.D.; Cho, K. Layered Molecular Ordering of Self-Organized Poly(3-Hexylthiophene) Thin Films on Hydrophobized Surfaces. *Macromolecules* **2006**, *39*, 5843–5847. [CrossRef]
12. Zhang, X.; Richter, L.J.; DeLongchamp, D.M.; Kline, R.J.; Hammond, M.R.; McCulloch, I.; Heeney, M.; Ashraf, R.S.; Smith, J.N.; Anthopoulos, T.D.; et al. Molecular Packing of High-Mobility Diketo Pyrrolo-Pyrrole Polymer Semiconductors with Branched Alkyl Side Chains. *J. Am. Chem. Soc.* **2011**, *133*, 15073–15084. [CrossRef]
13. Shen, X.; Hu, W.; Russell, T.P. Measuring the Degree of Crystallinity in Semicrystalline Regioregular Poly(3-Hexylthiophene). *Macromolecules* **2016**, *49*, 4501–4509. [CrossRef]
14. Verploegen, E.; Mondal, R.; Bettinger, C.J.; Sok, S.; Toney, M.F.; Bao, Z. Effects of Thermal Annealing Upon the Morphology of Polymer-Fullerene Blends. *Adv. Funct. Mater.* **2010**, *20*, 3519–3529. [CrossRef]
15. Peng, R.; Zhu, J.; Pang, W.; Cui, Q.; Wu, F.; Liu, K.; Wang, M.; Pan, G. Thermal Annealing Effects on the Absorption and Structural Properties of Regioregular Poly (3-Hexylthiophene) Films. *J. Macromol. Sci.* **2011**, *50*, 624–636. [CrossRef]
16. Gu, K.; Wang, Y.; Li, R.; Tsai, E.; Onorato, J.W.; Luscombe, C.K.; Priestley, R.D.; Loo, Y.-L. Role of Postdeposition Thermal Annealing on Intracrystallite and Intercrystallite Structuring and Charge Transport in Poly(3-Hexylthiophene). *ACS Appl. Mater. Interfaces* **2021**, *13*, 999–1007. [CrossRef]
17. Wang, T.; Pearson, A.J.; Lidzey, D.G.; Jones, R.A.L. Evolution of Structure, Optoelectronic Properties, and Device Performance of Polythiophene:Fullerene Solar Cells during Thermal Annealing. *Adv. Funct. Mater.* **2011**, *21*, 1383–1390. [CrossRef]
18. Singh, C.R.; Gupta, G.; Lohwasser, R.; Engmann, S.; Balko, J.; Thelakkat, M.; Thurn-Albrecht, T.; Hoppe, H. Correlation of Charge Transport with Structural Order in Highly Ordered Melt-Crystallized Poly(3-Hexylthiophene) Thin Films. *J. Polym. Sci. Part B Polym. Phys.* **2013**, *51*, 943–951. [CrossRef]
19. Joseph Kline, R.; McGehee, M.D.; Toney, M.F. Highly Oriented Crystals at the Buried Interface in Polythiophene Thin-Film Transistors. *Nat. Mater.* **2006**, *5*, 222–228. [CrossRef]
20. Malik, S.; Nandi, A.K. Crystallization Mechanism of Regioregular Poly(3-Alkyl Thiophene)s. *J. Polym. Sci. B Polym. Phys.* **2002**, *40*, 2073–2085. [CrossRef]
21. Sun, X.; Ren, Z.; Liu, J.; Takahashi, I.; Yan, S. Structure Evolution of Poly(3-Hexylthiophene) on Si Wafer and Poly(Vinylphenol) Sublayer. *Langmuir* **2014**, *30*, 7585–7592. [CrossRef]
22. Kim, D.H.; Jang, Y.; Park, Y.D.; Cho, K. Surface-Induced Conformational Changes in Poly(3-Hexylthiophene) Monolayer Films. *Langmuir* **2005**, *21*, 3203–3206. [CrossRef]
23. Ruffino, R.; Tuccitto, N.; Messina, G.M.L.; Kozma, E.; Catellani, M.; Li-Destri, G.; Marletta, G. Polymer Crystallization on Nanocurved Substrates: Distortion Versus Dewetting. *J. Phys. Chem. C* **2019**, *123*, 8967–8974. [CrossRef]

24. Ruffino, R.; Fichera, L.; Valenti, A.; Jankowski, M.; Konovalov, O.; Messina, G.M.L.; Licciardello, A.; Tuccitto, N.; Li-Destri, G.; Marletta, G. Tuning the Randomization of Lamellar Orientation in Poly(3-Hexylthiophene) Thin Films with Substrate Nano-Curvature. *Polymer* **2021**, *230*, 124071. [CrossRef]
25. Donose, B.C.; Taran, E.; Vakarelski, I.U.; Shinto, H.; Higashitani, K. Effects of Cleaning Procedures of Silica Wafers on Their Friction Characteristics. *J. Colloid Interface Sci.* **2006**, *299*, 233–237. [CrossRef]
26. Qu, Y.; Li, L.; Lu, G.; Zhou, X.; Su, Q.; Xu, W.; Li, S.; Zhang, J.; Yang, X. A Novel Melting Behavior of Poly(3-Alkylthiophene) Cocrystals: Premelting and Recrystallization of Component Polymers. *Polym. Chem.* **2012**, *3*, 3301–3307. [CrossRef]
27. Usov, I.; Mezzenga, R. FiberApp: An Open-Source Software for Tracking and Analyzing Polymers, Filaments, Biomacromolecules, and Fibrous Objects. *Macromolecules* **2015**, *48*, 1269–1280. [CrossRef]
28. Oyewole, D.O.; Oyewole, O.K.; Kushnir, K.; Shi, T.; Oyelade, O.V.; Adeniji, S.A.; Agyei-Tuffour, B.; Evans-Lutterodt, K.; Titova, L.V.; Soboyejo, W.O. Pressure and Thermal Annealing Effects on the Photoconversion Efficiency of Polymer Solar Cells. *AIP Adv.* **2021**, *11.4*, 045304. [CrossRef]
29. Ali, K.; Pietsch, U.; Grigorian, S. Enhancement of Field-Effect Mobility Due to Structural Ordering in Poly(3-Hexylthiophene) Films by the Dip-Coating Technique. *J. Appl. Crystallogr.* **2013**, *46*, 908–911. [CrossRef]
30. Son, S.Y.; Park, T.; You, W. Understanding of Face-On Crystallites Transitioning to Edge-On Crystallites in Thiophene-Based Conjugated Polymers. *Chem. Mater.* **2021**, *33*, 4541–4550. [CrossRef]
31. Joshi, S.; Grigorian, S.; Pietsch, U. X-ray Structural and Crystallinity Studies of Low and High Molecular Weight Poly(3-hexylthiophene). *Phys. Status Solidi A* **2008**, *205*, 488–496. [CrossRef]
32. Joshi, S.; Grigorian, S.; Pietsch, U.; Pingel, P.; Zen, A.; Neher, D.; Scherf, U. Thickness Dependence of the Crystalline Structure and Hole Mobility in Thin Films of Low Molecular Weight Poly(3-Hexylthiophene). *Macromolecules* **2008**, *41*, 6800–6808. [CrossRef]
33. Jiao, X.; Statz, M.; Lai, L.; Schott, S.; Jellett, C.; McCulloch, I.; Sirringhaus, H.; McNeill, C.R. Resolving Different Physical Origins toward Crystallite Imperfection in Semiconducting Polymers: Crystallite Size vs Paracrystallinity. *J. Phys. Chem. B* **2020**, *124*, 10529–10538. [CrossRef]
34. Mwema, F.M.; Akinlabi, E.T. The Use of Power Spectrum Density for Surface Characterization of Thin Films. In *book: Photoenergy and Thin Film Materials*; Yang, X.-Y., Ed.; John Wiley & Sons Inc: Hoboken, NJ, USA, 2019; Chapter 9, pp. 379–411.
35. Li Destri, G.; Keller, T.F.; Catellani, M.; Punzo, F.; Jandt, K.D.; Marletta, G. Crystalline Monolayer Ordering at Substrate/Polymer Interfaces in Poly(3-Hexylthiophene) Ultrathin Films. *Macromol. Chem. Phys.* **2011**, *212*, 905–914. [CrossRef]
36. Li Destri, G.; Keller, T.F.; Catellani, M.; Punzo, F.; Jandt, K.D.; Marletta, G. Interfacial Free Energy Driven Nanophase Separation in Poly(3-Hexylthiophene)/[6,6]-Phenyl-C61-Butyric Acid Methyl Ester Thin Films. *Langmuir* **2012**, *28*, 5257–5266. [CrossRef]